Chapter 5

Transition between coupling induced absorption and transparency

In this final technical chapter, we have developed a quantum theoretical framework for the hybrid quantum systems having multiple modes [Shrivastava et al., 2024a]. We use two types of modes, one having tunable properties (TM) while other modes are static (SM) in nature. We consider two cases: the first case having three modes, 1TM and 2SMs. When an individual SM is getting coupled with TM, level attraction (LA) is happening but when both SMs are getting coupled with TM we observe transition from LA to level repulsion (LR). The second case has four modes, 1TM and 3SMs. Again when individual SM is coupled with TM, LA is happening but when all SMs are getting coupled with TM the transition from LA to LR is happening. When the transition from LA to LR is happening in the midway of the transition, level absorption is also observed. Here for the two simple cases we achieved controllable transition from LA to LR in the multimode hybrid quantum system. By tuning the coupling parameters, different nature of transitions e.g. from LR to LA, LR to LR, LA to LA, LA or LR to level absorptions and vice versa may also be achieved [Hu et al., 2022; Rao et al., 2021b; Bhoi et al., 2022]. We have developed a general model explaining these phenomena, extending our findings for multiple modes having different hybrid quantum systems of N modes. Our analysis unveils the complex dynamics of the interaction between different modes of hybrid quantum systems. We expect a good understanding of these intricate mechanisms to advance the application for future quantum technologies. In the previous chapter we observed CIT and CIA using different geometries of resonators. In this chapter we present a mechanism where these phenomena can be interchanged by controlling the coupling between the resonators [Shrivastava et al., 2024a].

5.1 Analytical modeling

To engineer the nature of coherent and dissipative coupling between different modes of the hybrid system connected to a channel in the form of bath / cavity / microstripline etc. to inject travelling photons in the system. The channel is also attached to input and output ports. We may write a general Hamiltonian for such a system as [Tiwari et al., 2024; Rao et al., 2020; Harder et al., 2021; Walls and Milburn, 2008; Scully and Zubairy, 1997b; Shrivastava et al., 2024b]

$$H/\hbar = \sum_{l=1}^{N}(\omega_l - i\alpha_l)\hat{X}_l^{\dagger}\hat{X}_l + \sum_{1\le l<m\le N}\Delta_{lm}(\hat{X}_l + \hat{X}_l^{\dagger})(\hat{X}_m + \hat{X}_m^{\dagger}) + \int \omega_k \hat{p}_k^{\dagger}\hat{p}_k dk + \int \left[\sum \lambda_l(\hat{X}_l + \hat{X}_l^{\dagger})(\hat{p}_k + \hat{p}_k{}^{\dagger})\right] dk. \tag{5.1}$$

After taking rotating wave approximation (RWA) we may write Eq. 5.1 as

$$H/\hbar = \sum_{l=1}^{N}(\omega_l - i\alpha_l)\hat{X}_l{}^{\dagger}\hat{X}_l + \sum_{1\le l<m\le N}\Delta_{lm}(\hat{X}_l\hat{X}_m^{\dagger} + \hat{X}_m\hat{X}_l^{\dagger}) + \int \omega_k \hat{p}_k{}^{\dagger}\hat{p}_k dk + \int \left[\sum \lambda_l(\hat{X}_l\hat{p}_k{}^{\dagger} + \hat{X}_l{}^{\dagger}\hat{p}_k)\right] dk. \tag{5.2}$$

Here l is the number of modes in the system which is varying from 1 to N, $\hat{X}_l^{\dagger}(\hat{X}_l)$ is the creation (annihilation) operators of the mode l. ω_l denote the resonance frequencies while α_l denote the intrinsic damping rate of the uncoupled mode l, the coupling parameter between different modes l and m are denoted by $\Delta_{lm} = J_{lm} + i\Gamma_{lm}$ where J_{lm} and Γ_{lm} are real parameters that characterize the strength of coherent and dissipative interactions between the modes l and m.

The third term of the Hamiltonian represents the feeding channel (cavity / bath / microstripline etc. as the case may be) connected to the input and output ports. In our formulation of Hamiltonian, we have modelled the feeding channel through which traveling photons mediate the interaction, integrating over a real domain from $-\infty$ to $+\infty$. Bosonic creation (annihilation) operator of the traveling photon is denoted by $\hat{p}_k^{\dagger}(\hat{p}_k)$ which obeys $[\hat{p}_k, \hat{p}_{k'}^{\dagger}] = \delta(k - k')$. ω_k denotes the frequency of travelling photon where k represents the wave vector. The last term represents the interaction between each mode and traveling photons, the interaction strength between travelling photon and each mode (from $l = 1$ to $l = N$) is denoted by λ_l, modelled linearly in $\hat{p}_k^{\dagger}(\hat{p}_k)$.

Following standard input output formalism the time forwarded Heisenberg-Langevin equations (subsection 4.1.2) of the l-th mode of the coupled system reads,

$$\dot{\hat{X}}_l(t) = -i\tilde{\omega}_l\hat{X}_l(t) - \beta_l\hat{X}_l(t) - i\sqrt{\beta_l}\hat{P}_{in}(t) - \sum_{\substack{m=1\\m\neq l}}^{N}\sqrt{\beta_l\beta_m}\hat{X}_m(t) - i\sum_{\substack{m=1\\m\neq l}}^{N}\Delta_{lm}\hat{X}_m(t) \tag{5.3}$$

where $\tilde{\omega}_l = \omega_l - i\alpha_l$, $\beta_l = 2\pi\lambda_l^2$ and $\beta_m = 2\pi\lambda_m^2$ represent the extrinsic damping rates of the mode l and m respectively. Here $\hat{P}_{in}$ ($\hat{P}_{out}$) is defined as the input (output) fields operator at the input (output) fields respectively. We observe that the external damping rates (β's) not only cause additional damping on top of the internal dissipation of respective components, but also cause the coupling between the components to become dissipative. After applying the Fourier transform the frequency domain equation may be written as [Hu et al., 2022; Shrivastava et al., 2024b; Rao et al., 2020]

$$\begin{aligned} &i(\omega-\tilde{\omega}_l)\hat{X}_l(\omega) - \beta_l\hat{X}_l(\omega) - i\sqrt{\beta_l}\hat{P}_{in}(\omega) \\ &\quad - \sum_{\substack{m=1\\m\neq l}}^{N}\sqrt{\beta_l\beta_m}\hat{X}_m(\omega) - i\sum_{\substack{m=1\\m\neq l}}^{N}\Delta_{lm}\hat{X}_m(\omega) = 0 \end{aligned} \tag{5.4}$$

Similarly, the time retarted Heisenberg-Langevin equation (subsection 4.1.2) of the coupled system in the time and frequency domain reads

$$\begin{aligned} \dot{\hat{X}}_l(t) = &-i\tilde{\omega}_l\hat{X}_l(t) + \beta_l\hat{X}_l(t) - i\sqrt{\beta_l}\hat{P}_{out}(t) \\ &+ \sum_{\substack{m=1\\m\neq l}}^{N}\sqrt{\beta_l\beta_m}\hat{X}_m(t) - i\sum_{\substack{m=1\\m\neq l}}^{N}\Delta_{lm}\hat{X}_m(t) \end{aligned} \tag{5.5}$$

$$\begin{aligned} &i(\omega-\tilde{\omega}_l)\hat{X}_l(\omega) + \beta_l\hat{X}_l(\omega) - i\sqrt{\beta_l}\hat{P}_{out}(\omega) \\ &\quad + \sum_{\substack{m=1\\m\neq l}}^{N}\sqrt{\beta_l\beta_m}\hat{X}_m(\omega) - i\sum_{\substack{m=1\\m\neq l}}^{N}\Delta_{lm}\hat{X}_m(\omega) = 0 \end{aligned} \tag{5.6}$$

We need to figure out the algebraic relation between the input and output port variables in order to derive the transmission results. From Eqs. 5.4 and Eqs. 5.6 we can get the input and

output field relation as

$$\hat{P}_{out}(\omega) = \hat{P}_{in}(\omega) - 2i\sum_{i=1}^{N}\sqrt{\beta_l}\hat{X}_l(\omega) \tag{5.7}$$

For CIT/CIA profile we numerically or experimentally measure the transmission coefficient S_{21} between input and output port of the hybrid system, which is defined as

$$S_{21} = \frac{\hat{p}_{out}}{\hat{p}_{in}} - 1 \tag{5.8}$$

Solving Eqs. 5.4, 5.7, and 5.8 numerically gives the transmission profile. S_{21} may also be written in matrix form as follows

$$S_{21} = \mathscr{B}^T \mathscr{M}^{-1} \mathscr{B} \tag{5.9}$$

where

$$\mathscr{B} = \sqrt{2}\begin{bmatrix} \sqrt{\beta_1} \\ \sqrt{\beta_2} \\ . \\ . \\ . \\ \sqrt{\beta_N} \end{bmatrix}_{N\times 1} ,$$

$$\mathscr{M} = i\begin{bmatrix} \omega - \tilde{\tilde{\omega}}_1 & -\Delta_{12} + i\sqrt{\beta_1\beta_2} & . & . & . & -\Delta_{1N} + i\sqrt{\beta_1\beta_N} \\ -\Delta_{12} + i\sqrt{\beta_1\beta_2} & \omega - \tilde{\tilde{\omega}}_2 & . & . & . & -\Delta_{2N} + i\sqrt{\beta_2\beta_N} \\ . & . & . & . & . & . \\ . & . & . & . & . & . \\ . & . & . & . & . & . \\ -\Delta_{1N} + i\sqrt{\beta_1\beta_N} & -\Delta_{2N} + i\sqrt{\beta_2\beta_N} & . & . & . & \omega - \tilde{\tilde{\omega}}_N \end{bmatrix}_{N\times N}$$

also $\Delta_{lm} = \Delta_{ml}$, and $\tilde{\tilde{\omega}}_l = \tilde{\omega}_l - i\beta_l = \omega_l - i(\alpha_l + \beta_l)$.

As a concrete example we are assuming TM to be made of magnon mode, magnon being collective spin excitation of ferromagnetic/antiferromagnetic material, resonance frequency of which can be tuned by applying external magnetic field. We may choose some magnetic thin film (e.g. yttrium iron garnet (YIG)) for excitation of the magnon mode, representative transmission profile is shown in the Fig. 1.2(a). Similarly for SM modes we may opt for photonic resonators (e.g. split ring resonator (SRR) / inverted split ring resonator

(ISRR)) resonance frequencies of which will remain constant with the applied magnetic field. Transmission profile is shown in the Fig. 1.2(a) for one photonic mode. Fig. 1.2(c) shows the case when there is no coupling between the photonic and magnonic modes.

5.2 Three mode coupled hybrid quantum systems

The physical systems realizing this generalized model are typically composed of components with very different underlying physics and coupling mechanisms. The effective modes that appear in such systems are called hybrid modes. For example, in this section we are dealing with two photonic resonators made of copper, and one magnonic resonator made of antiferromagnetic material yttrium-iron-garnet (YIG). Since, the properties of the photonic resonators are not going to change with applied magnetic fields, we are saying this static mode. On the other hand the properties of YIG are changing with applied magnetic field, we are referring to it as tunable mode. The simplest case where a transition between CIT and CIA is possible without changing the nature of any coupling, is that of three modes. For simplicity we consider one of the modes to be tunable while the other two as static. Schematic of such an experiment is shown in Fig. 5.1, where the tunable mode we are taking as magnon (YIG) that we are denoting by M, whose resonance frequency can be tuned by applying an external magnetic field. Static modes are made out of ISSRs, whose resonance frequencies will remain unaffected by the applied external magnetic field. The two static modes are two different ISRRs of different dimensions, having different resonance frequencies. The feedline in this planar structure is a microstripline (MSL) common to both type of modes, the MSL in turn is also attached to the input and output port of vector network analyzer (VNA), from where microwave photons are getting injected into the system that are initiating and creating all of the dynamics.

5.2.1 Model and analysis

We have modelled the three mode coupled photon-magnon hybrid quantum system using the Hamiltonian of Eq. 5.2 by restricting it to 1 magnon (M) and 2 photon modes P_1 and P_2 [Hu et al., 2022; Tiwari et al., 2024; Rao et al., 2020; Harder et al., 2021; Walls and Milburn,

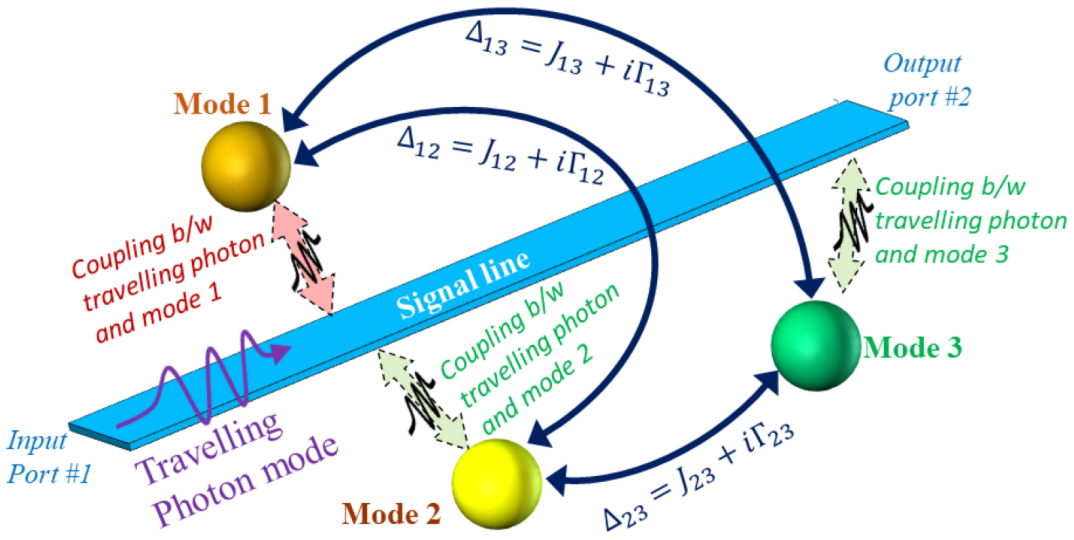

Fig. 5.1 Cartoon showing a simple planar hybrid system having three modes, out of which mode 1 (M) is tunable, and mode 2 (P_1) and mode 3 (P_2) are static modes. For tuning of M we have applied an external inplane static magnetic field perpendicular to the feedline (MSL).

2008; Scully and Zubairy, 1997a; Shrivastava et al., 2024b]

$$
\begin{aligned}
H_{(M,P_1,P_2)}/\hbar = {} & \tilde{\omega}_M \hat{X}_M^\dagger \hat{X}_M + \tilde{\omega}_{P_1} \hat{X}_{P_1}^\dagger \hat{X}_{P_1} + \tilde{\omega}_{P_2} \hat{X}_{P_2}^\dagger \hat{X}_{P_2} + \int \omega_k \hat{p}_k^\dagger \hat{p}_k dk \\
& + \Delta_{MP_1} (\hat{X}_M \hat{X}_{P_1}^\dagger + \hat{X}_{P_1} \hat{X}_M^\dagger) + \Delta_{MP_2} (\hat{X}_M \hat{X}_{P_2}^\dagger + \hat{X}_{P_2} \hat{X}_M^\dagger) + \Delta_{P_1P_2} (\hat{X}_{P_1} \hat{X}_{P_2}^\dagger + \hat{X}_{P_2} \hat{X}_{P_1}^\dagger) \\
& + \int \left[\lambda_M (\hat{X}_M \hat{p}_k^\dagger + \hat{X}_M^\dagger \hat{p}_k) + \lambda_{P_1} (\hat{X}_{P_1} \hat{p}_k^\dagger + \hat{X}_{P_1}^\dagger \hat{p}_k) + \lambda_{P_2} (\hat{X}_{P_2} \hat{p}_k^\dagger + \hat{X}_{P_2}^\dagger \hat{p}_k) \right] dk,
\end{aligned}
\tag{5.10}
$$

where $\tilde{\omega}_M = \omega_M - i\alpha_M$, $\tilde{\omega}_{P_1} = \omega_{P_1} - i\alpha_{P_1}$ and $\tilde{\omega}_{P_2} = \omega_{P_2} - i\alpha_{P_2}$ are the complex frequencies of the magnon M and photon modes P_1 and P_2 respectively. Here α_M , α_{P_1} and α_{P_2} are intrinsic damping parameters for the M, P_1 and P_2 modes respectively . It is a well established fact that LA or LR is determined by the relative and combined strength and phase of the oscillating magnetic fields generated from ISRRs split gap, magnon and the travelling waves of MSL. Also for coherent coupling (LR) the complex coupling constant ($\Delta = J + i\Gamma$) has a dominating real part (J) and for dissipative coupling (LA) it has a dominating imaginary part (Γ).

The Heisenberg-Langevin equations for this system can be compactly written in a matrix form as

$$\frac{d}{dt}\begin{bmatrix}\hat{X}_M\\ \hat{X}_{P_1}\\ \hat{X}_{P_2}\end{bmatrix} = -iH_{coupling}\begin{bmatrix}\hat{X}_M\\ \hat{X}_{P_1}\\ \hat{X}_{P_2}\end{bmatrix} - i\begin{bmatrix}\sqrt{\beta_M}\\ \sqrt{\beta_{P_1}}\\ \sqrt{\beta_{P_2}}\end{bmatrix}\hat{P}_{in}(t) \tag{5.11}$$

where,

$$H_{coupling} = \begin{bmatrix} \tilde{\tilde{\omega}}_M & \Delta_{MP_1} - i\sqrt{\beta_M\beta_{P_1}} & \Delta_{MP_2} - i\sqrt{\beta_M\beta_{P_2}} \\ \Delta_{MP_1} - i\sqrt{\beta_M\beta_{P_1}} & \tilde{\tilde{\omega}}_{P_1} & \Delta_{P_1P_2} - i\sqrt{\beta_{P_1}\beta_{P_2}} \\ \Delta_{MP_2} - i\sqrt{\beta_M\beta_{P_2}} & \Delta_{P_1P_2} - i\sqrt{\beta_{P_1}\beta_{P_2}} & \tilde{\tilde{\omega}}_{P_2} \end{bmatrix}$$

where, β_M, β_{P_1}, β_{P_2} are external damping rates for the M, P_1 and P_2 modes respectively and $\Delta_{lm} = \Delta_{ml}$ and $\tilde{\tilde{\omega}}_l = \tilde{\omega}_l - i\beta_l = \omega_l - i(\alpha_l + \beta_l)$. Therefore the complex frequencies of the modes after taking into account the internal damping and coupling induced (external) damping may be written as $\tilde{\tilde{\omega}}_M = \omega_M - i(\alpha_M + \beta_M)$, $\tilde{\tilde{\omega}}_{P_1} = \omega_{P_1} - i(\alpha_{P_1} + \beta_{P_1})$, $\tilde{\tilde{\omega}}_{P_2} = \omega_{P_2} - i(\alpha_{P_2} + \beta_{P_2})$ for magnon mode (M), photon modes P_1 and P_2 respectively. Whenever the direct interaction between magnon and the two photon modes happens, the resonance frequencies of the hybridised modes are splitted into higher and lower branches for LR and get merged around coupling center for LA, that can be analytically solved by using coupling matrix ($H_{coupling}$) of the Eq. 5.11 for real parts of its eigenvalues.

The input and output port variables are related to each other. In this case using Eq. 5.7, for 3 modes we can write P_{out} and P_{in} relation in frequency domain as [Rao et al., 2020; Hu et al., 2022; Shrivastava et al., 2024b]

$$\hat{P}_{out}(\omega) - \hat{P}_{in}(\omega) = -2i\left[\sqrt{\beta_M}\hat{X}_M(\omega) + \sqrt{\beta_{P_1}}\hat{X}_{P_l}(\omega) + \sqrt{\beta_{P_2}}\hat{X}_{P_2}(\omega)\right] \tag{5.12}$$

For calculating the dispersion spectra of different types of cooperative effect taking into account all the interactions of magnon mode, photon modes and travelling photon modes of the combined hybrid system first we need to calculate S_{21} (on $\frac{\omega}{2\pi} - H_{dc}$ plane), which is the numerically simulated and experimentally measured parameter between input and output ports. Following Eq. 5.8 this can be written for 1 magnon and 2 photon modes as

$$S_{21} = \frac{\hat{P}_{out}}{\hat{P}_{in}} - 1 = -\frac{2i}{\hat{P}_{in}}\left[\sqrt{\beta_M}\hat{X}_M + \sqrt{\beta_{P_1}}\hat{X}_{P_l} + \sqrt{\beta_{P_2}}\hat{X}_{P_2}\right] \tag{5.13}$$

The transmission profile in matrix form for 3 modes is given by Eq. 5.9 with

$$S_{21} = \mathscr{B}^T_{1\times 3}\mathscr{M}^{-1}_{3\times 3}\mathscr{B}_{3\times 1} \tag{5.14}$$

where

$$\mathscr{B} = \sqrt{2}\begin{bmatrix} \sqrt{\beta_M} \\ \sqrt{\beta_{P_1}} \\ \sqrt{\beta_{P_2}} \end{bmatrix},$$

$$\mathscr{M} = i\begin{bmatrix} \omega - \tilde{\tilde{\omega}}_M & -\Delta_{MP_1} + i\sqrt{\beta_M\beta_{P_1}} & -\Delta_{MP_2} + i\sqrt{\beta_M\beta_{P_2}} \\ -\Delta_{MP_1} + i\sqrt{\beta_M\beta_{P_1}} & \omega - \tilde{\tilde{\omega}}_{P_1} & -\Delta_{P_1P_2} + i\sqrt{\beta_{P_1}\beta_{P_2}} \\ -\Delta_{MP_2} + i\sqrt{\beta_M\beta_{P_2}} & -\Delta_{P_1P_2} + i\sqrt{\beta_{P_1}\beta_{P_2}} & \omega - \tilde{\tilde{\omega}}_{P_2} \end{bmatrix}.$$

5.2.2 Results and discussion

The transmission properties of the system are studied using vector network analyzer which sends microwave photons of frequency $f_{AC} = \omega/2\pi$ through the feeding line MSL for different strengths of applied static magnetic field H_{dc}. Fig. 5.2(a) shows S_{21} power spectra of the two ISRRs without YIG film, where only two transmission lines horizontal to the applied H_{dc} having resonance frequencies ω_{P_1}= 3.4, ω_{P_2}= 4.1 GHz with intrinsic damping rates α_{P_1}=0.002, and α_{P_1}=0.002 respectively [Bhoi et al., 2022; Bernier et al., 2018; Hu et al., 2022; Rao et al., 2020; Harder et al., 2021] are visible in the transmission profile on the $(H_{dc} - f_{AC})$ plane which is unaffected by the tuned magnetic field. Fig. 5.2(b) shows S_{21} power spectra of the YIG film without the ISRRs, showing magnon excitations in the YIG films termed as ferromagnetic resonance (FMR) mode having intrinsic damping rate α_M=0.00002 [Bhoi et al., 2022; Bernier et al., 2018; Hu et al., 2022; Rao et al., 2020; Harder et al., 2021], visible as a slant transmission line which is getting tuned by the applied H_{dc} ranging from 0.0 to 3.0 kOe. Resonance frequency of this FMR mode can be linearly modelled as $\omega_M = 0.714 \times H_{dc} + 2.714$ which is varying from 2.714 to 4.856 GHz. Fig. 5.2(c) shows S_{21} power spectra of the two ISRRs and YIG film in absence of any coupling, which simply gives the addition of Fig. 5.2(a) and (b) and transmission line of magnon just crosses the transmission lines of photons.

When YIG gets excited and its FMR mode interacts with P_1 and P_2 modes with some strength of coupling parameter, its effects will be reflected in the transmission profile. When only M and P_1 interact with the coupling parameter $\Gamma_{MP_1} = 0.1i$ there will be LA. Similarly when only M and P_2 interact with coupling parameter $\Gamma_{MP_2} = 0.1i$ there will also be LA near the respective resonance frequencies of the coupling center of the coupled pair for MP_1 at 3.4 GHz and MP_2 at 4.1 GHz respectively as shown in Fig. 5.2(d). Fig. 5.2(e) shows the real part of the complex eigenfrequencies of the state of the system discussed in the Fig. 5.2(d). This shows two clear and distinct LAs, one for the MP_1 where higher and lower eigenfrequency branches are getting merged and then separated, another one for the MP_2 where again higher

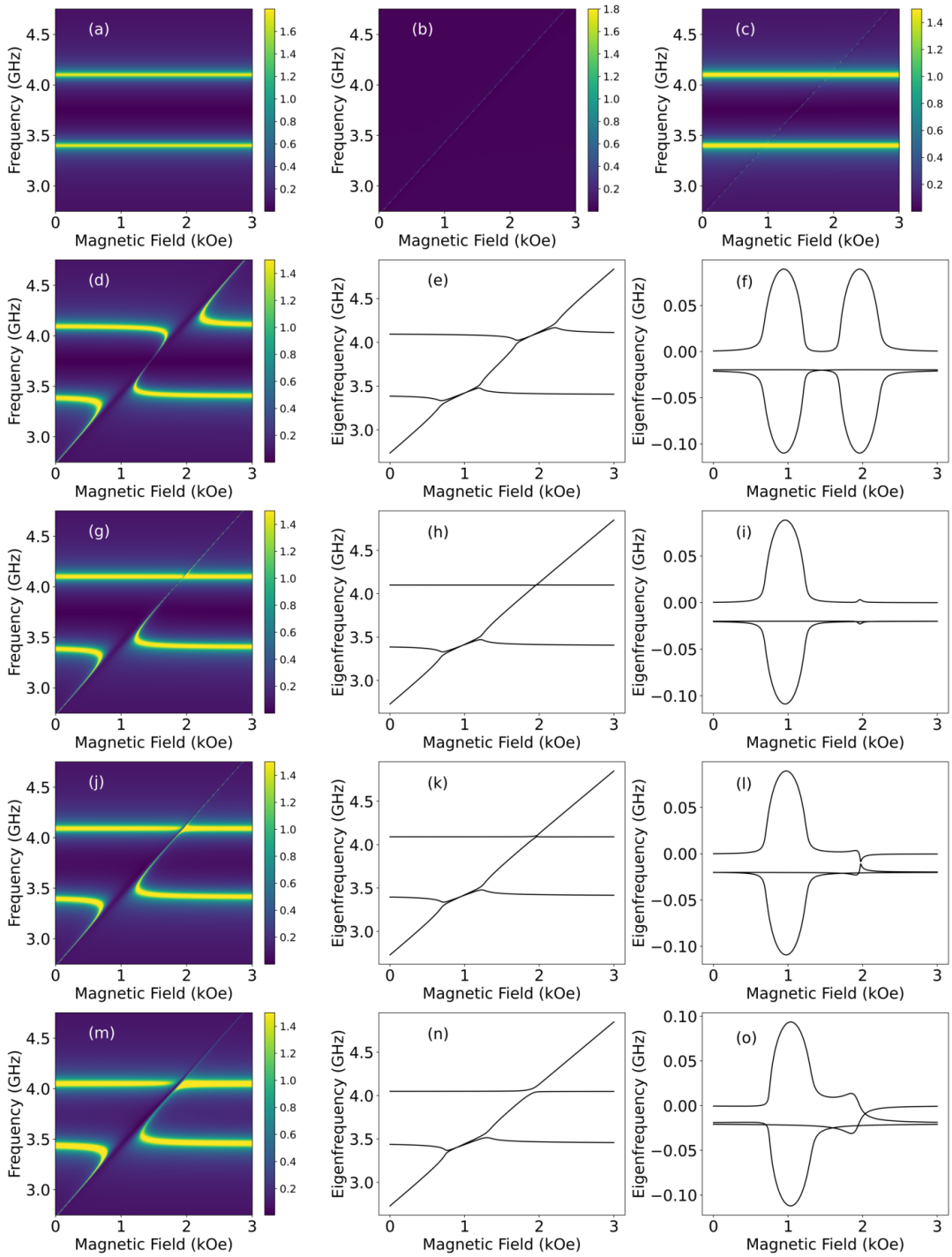

Fig. 5.2 (Caption on next page.)

Fig. 5.2 (a) Transmission profile for two static modes, (b) transmission profile for magnon mode, (c) combined transmission profile for two static modes and magnonic mode without any coupling. Hybrid quantum system having 1 TM coupled individually to 2 SMs. Fig(d) Transmission profile, (e) real, and (f) Imaginary part of complex eigenfrequencies, with no coupling between individual SMs. (g) Transmission profile; (h) Real, and (i) imaginary part of complex eigenfrequencies, when coupling parameter between SMs is $0.01i$. (j) Transmission profile; (k) Real, and (l) imaginary part of complex eigenfrequencies, when coupling parameter between SMs is $0.1i$. (m) Transmission profile; (n) Real, and (o) imaginary part of complex eigenfrequencies, when coupling parameter between SMs is $0.2i$. The change of parameters are summarized in Table 5.1

and lower eigenfrequency branches are getting merged and then separated. In these two cases of LAs the lower and upper branches of the hybridised modes are getting attracted and merging to a common eigenfrequency near the coupling center with comparatively strong microwave absorption, resulting in an anti crossing called CIA.

In the hybrid system multiple interaction paths between the travelling waves of MSL, magnon mode and two photon modes are giving rise to the phenomenon of LA and LR. Fig. 5.2(d,e) shows the decoupled case between the photonic modes (i.e. $\Delta_{P_1P_2} = 0$). The travelling microwave photons are reaching the different photonic modes and the magnonic mode is getting directly coupled with the two photonic modes, resulting in further interaction with the travelling photon modes of MSL. In this way the hybrid coupling modification with the travelling waves of photon modes will determine the type of interactions, LA or LR etc.

For the first part of coupled hybrid system when we are considering interactions between M and P_1, their dispersion [Fig. 5.2(d)] and real part of their eigenvalue [Fig. 5.2(e)] are in good agreement for the LA at 3.4 GHz with internal and external dissipation 0.00002 and 0.00018 (0.002 and 0.018) [Bhoi et al., 2022; Bernier et al., 2018; Hu et al., 2022; Rao et al., 2020; Harder et al., 2021] for magnon (photon 1) mode respectively. The internal and external dissipations for Fig. 5.2(d-o) are going to be constant throughout the discussions.

In Fig. 5.2(f) we have drawn the imaginary part of complex eigenvalues solution of $H_{coupling}$ for MP_1 and MP_2. For MP_1 first part of Fig. 5.2(e, h, k, n) are real part of their complex eigenvalues that also correspond to the first part of transmission profile Fig. 5.2(d, g, j, m) respectively and showed LA. Repulsive nature in linewidth for Fig. 5.2(f, i, l, o) confirms dissipative coupling (CIA) having the coupling constant $\Delta_{MP_1} = 0.1i$ for the first part of the Fig. 5.2(d-o). The coupling constant $\Delta_{MP_1} = 0.1j$ corresponds to the Fig. 5.2(d, e, f), where Fig. 5.2(d, e) shows lower / higher frequency branches of the corresponding hybrid modes. These two modes are merged near coupling center because of CIT phenomenon by virtue of imaginary coupling parameter. Fig. 5.2(d, g, j, m) representing transmission

Subplots	Δ_{MP_2}	$\Delta_{P_1P_2}$	Eigenvalues near MP_2 crossing	
			Real part	imaginary part
d-f	0.1i	0i	Attraction	Repulsion
g-i	0.01i	0.01i	Intermediate	Repulsion
j-l	0.01i	0.1i	Intermediate	intermediate
m-o	0.02i	0.2i	Repulsion	Attraction

Table 5.1 Set of parameters that are changing and the eigenvalues which are changing qualitatively in Fig. 5.2

profiles and their corresponding real and imaginary parts of complex eigenvalue are shown in Fig. 5.2(f, i, l, o) respectively.

We now considers interactions between M and P_2 in second part of the coupled hybrid system taking coupling constant $\Delta_{MP_2} = 0.1i$ correspond to the Fig. 5.2(d,e) where lower/higher branches of the frequency corresponds to the hybrid modes, the two modes are merged near coupling center because of CIA effects by having imaginary coupling parameter between M and P_2 with no coupling between P_1 and P_2. The dispersion profiles shown in Fig. 5.2(d, g, j, m) and real part of their eigenvalues Fig. 5.2(e, h, k, n) well agrees for each at 3.7 GHz with internal and external dissipation 0.00002 and 0.00018 (0.002 and 0.018) for magnon (photon 2) mode [Bhoi et al., 2022; Bernier et al., 2018; Hu et al., 2022; Rao et al., 2020; Harder et al., 2021] respectively. The internal and external dissipations for MP_2 are going to be constant throughout the discussion.

The coupling constant between M and P_2 for the third row Fig. 5.2(g, h, i) is $\Delta_{MP_2} = 0.01i$ and the inter-photonic coupling constant is $\Delta_{P_1P_2} = 0.01i$ between P_1 and P_2. Fig. 5.2 (g,h) shows lower / higher branches of the eigenfrequencies corresponding to the hybrid modes. These coupled modes are crossing near coupling center implying CIA phenomenon but now having a less imaginary coupling parameter. In Fig. 5.2(i) we have drawn imaginary part of the complex eigenvalues of the coupling matrix, for MP_2 showing that the repulsion in their linewidth at the coupling centre have reduced considerably compared to the case Fig. 5.2(f). The coupling constant between M and P_2 for the fourth row Fig. 5.2(j, k, l) is $\Delta_{MP_2} = 0.01i$ with inter-photonic coupling constant is $\Delta_{P_1P_2} = 0.1i$ between P_1 and P_2. Fig. 5.2(j,k) shows lower / higher frequency branches of the corresponding hybrid modes, these two modes are still crossing near coupling center and still confirming CIA phenomenon by virtue of a reduced imaginary coupling strength despite of increasing inter-photonic coupling constant. In Fig. 5.2(l) we have drawn imaginary part of the eigenvalues of $H_{coupling}$ for MP_2, in their linewidth the repulsion diminishes and it is just to start attraction/ crossing but have not started yet, this behaviour still confirms CIA. The coupling constant between M and P_2

for the fifth row Fig. 5.2(m, n, o) is $\Delta_{MP_2} = 0.02i$ and inter-photonic coupling constant is $\Delta_{P_1P_2} = 0.2i$ between P_1 and P_2. Fig. 5.2(m,n) shows lower/higher frequency branches of the coupled hybrid modes with no attraction in the levels but they remain separated near coupling center that clearly confirms CIT phenomenon that is combined effect of Δ_{MP_2} and $\Delta_{P_1P_2}$, which is now twice the value from the previous row Fig. 5.2(j, k, l). In Fig. 5.2(l) we have drawn the imaginary part of eigenfrequencies of $H_{coupling}$, showing clear attraction in their linewidth as they are crossing each other.

The observation of CIA(LA) and CIT(LR) may be described as a balance between the multiple interaction possibilities between the magnon mode, photon modes and travelling photons. In the region where magnon mode and first photon mode are getting coupled around 3.4 GHz, their respective internal dissipation and external dissipation are constant, these parameters are not going to play much role in the transition of the behaviour. Also coupling parameter between M and P_1 i.e. Δ_{MP_1} is not changing from second to fifth row so its behaviour in transmission profile and in real or imaginary parts of eigenvalues is also not getting affected, although coupling parameters between M and P_2 i.e. Δ_{MP_2} and P_1P_2 i.e. $\Delta_{P_1P_2}$ are changing but the effective contribution of Δ_{MP_2} and $\Delta_{P_1P_2}$ are interfering destructively and the property of MP_1 interactions remains unaffected.

For the region where magnon mode and second photon mode is getting coupled around 3.7 GHz, their respective internal and external dissipation and the coupling parameter between M and P_1 i.e. Δ_{MP_1} being constant, so these parameters are not going to play much role in the transition of their behaviour. So the rest of the coupling parameters, namely Δ_{MP_2} and $\Delta_{P_1P_2}$ are dominantly and effectively playing the role in the transition phenomenon. For the Fig. 5.2(d, e, f) $\Delta_{MP_2} = 0.1i$ and $\Delta_{P_1P_2} = 0$ so transmission profile, Fig. 5.2(d), and real part of eigenvalue, Fig. 5.2(e), both show CIA (LA), and their linewidth profile (imaginary part of complex eigenvalue), Fig. 5.2(f), shows repulsion.

For the Fig. 5.2(g, h, i) $\Delta_{MP_2} = 0.01i$ and $\Delta_{P_1P_2} = 0.01i$ so transmission profile and real part of eigenvalue Fig. 5.2(g, h) respectively shows CIA while levels are just crossing, but their linewidth profile (imaginary part of complex eigenvalue) Fig. 5.2(i) shows very small reminisces of linewidth repulsion. So here for the Fig. 5.2(g, h, i) Δ_{MP_2} and $\Delta_{P_1P_2}$ are dominating in such a way that level attraction approximately diminishes to level absorption which is clearly visible in Fig. 5.2(g, h) and also minutely visible in Fig. 5.2(i). For the Fig. 5.2(j, k, l) $\Delta_{MP_2} = 0.01i$ and $\Delta_{P_1P_2} = 0.1$ so the transmission profile and real part of eigenvalue, Fig. 5.2(j, k), respectively shows CIA behaviour while levels are still just crossing, but their linewidth profile, Fig. 5.2(l), totally diminishes LR behaviour and starts towards attracting the linewidth but still it is just about to cross. So here for the Fig. 5.2(j, k, l) Δ_{MP_2} and $\Delta_{P_1P_2}$ are dominating in such a way that level attraction is diminished to level absorption

which is clearly visible in Fig. 5.2(g, h) and also the signature of linewidth attraction which is just about to touch is visible in Fig. 5.2(i). The outcomes of Fig. 5.2(g, h, i) and Fig. 5.2(j, k, l) signifies a special phenomenon known as level absorption which is visible in the midway when transition between level attraction to repulsion is happening.

For the Fig. 5.2(m, n, o) $\Delta_{MP_2} = 0.02i$ and $\Delta_{P_1P_2} = 0.2$. The transmission profile and real part of eigenvalue, Fig. 5.2(m, n), signifies CIT while levels are getting closer but remains splitted between higher and lower branches near the crossing center. Also in their linewidth profile, Fig. 5.2(o), attraction in linewidth is clear as they are crossing each other. So here for the Fig. 5.2(m, n, o), Δ_{MP_2} and $\Delta_{P_1P_2}$ are dominating in such a way that a clear coupling induced transparency appears in the Fig. 5.2(m, n) and also the a clear attraction in linewidth or crossing is visible in Fig. 5.2(o).

In the case of coherent coupling (LR/CIT) the frequencies of hybridised mode are repelling each other and their linewidths are crossing, but in the case of dissipative coupling (LA/CIA) the trends become opposite, i.e. frequencies of hybridised mode are attracting each other and their linewidths are repelling. But when system is undergoing transition from coherent to dissipative coupling or vice versa at the point when transition is happening the frequencies of hybridised modes are just crossing. Still it is characterised under coupling induced absorption but it is similar to the case when there is no coupling between the modes or there is very little coupling. So only by looking at the transmission and real part of eigenvalue profile it is hard to distinguish but even in this situation of CIA where levels are just crossing each other the existence of strong coupling near the coupling center signifies the phenomenon leading to blocking/ absorption of microwave transmission and also their linewidth profile branches still should be repulsive even for a narrow range of field, and these two features distinguishes this transition point from weakly coupled or not coupled hybrid modes. Therefore in a multimode hybrid system the behaviour of the pair of modes under consideration not only depends on their parameters but may get influenced by the presence of other modes of the system too.

5.3 Four modes coupled hybrid quantum systems

This section is a relatively straightforward extension of the previous section with one more static mode motivated by a recent experiment [Bhoi et al., 2022]. Here in total we have taken one tunable mode and three static modes in a planar hybrid structure. Schematic of the experiment is shown in Fig. 5.3. As discussed in the previous section for tunable mode we are taking a magnon (YIG) that we are denoting by M, whose resonance frequency can be tuned by applying an external magnetic field. Static modes are photonic in nature and

made of ISSRs, whose resonance frequencies are unaffected by the applied external magnetic field. For the three static modes we make three different ISRRs of different dimensions having different resonance frequencies. Like before the input and output ports of the VNA are attached to the MSL of the hybrid system through which microwave photons are getting injected into the system that are initiating and creating all of the dynamics.

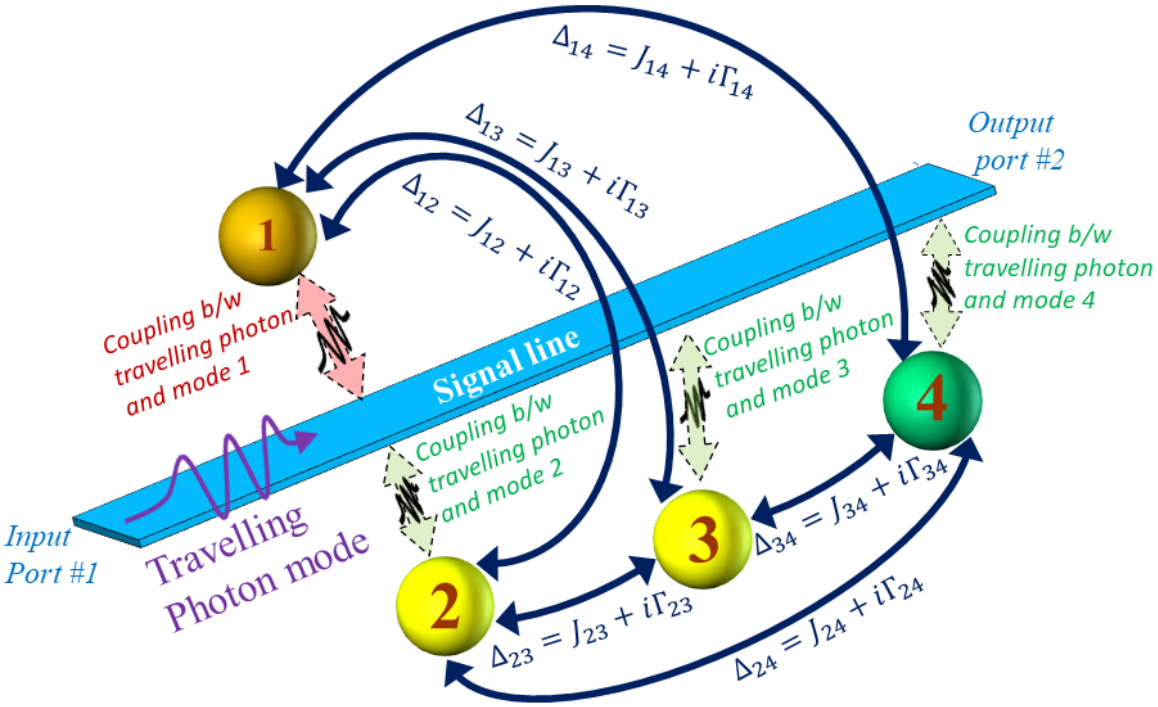

Fig. 5.3 Cartoon showing a simple planar hybrid system having 4 modes, out of which mode 1 (M) is tunable and mode 2 (P_1), mode 3 (P_2) and mode 4 (P_3) are static modes. For tuning of M we have applied an in- plane static magnetic field perpendicular to the feedline/signal-line.

5.3.1 Model and analysis

After taking rotating wave approximation (RWA) we may write Eq. 5.1 for four modes as [Hu et al., 2022; Tiwari et al., 2024; Rao et al., 2020; Harder et al., 2021; Walls and Milburn, 2008; Scully and Zubairy, 1997a; Shrivastava et al., 2024b]

$$H/\hbar = \sum_{l=1}^{4}(\omega_l - i\alpha_l)\hat{X_l}^{\dagger}\hat{X_l} + \sum_{1\le l<m\le N}\Delta_{lm}(\hat{X_l}\hat{X_m}^{\dagger} + \hat{X_m}\hat{X_l}^{\dagger}) + \int \omega_k \hat{p_k}^{\dagger}\hat{p_k}dk + \int \left[\sum \lambda_l(\hat{X_l}\hat{p_k}^{\dagger} + \hat{X_l}^{\dagger}\hat{p_k})\right]dk \tag{5.15}$$

where different symbols have their usual meaning as described in the previous section except one extension that here we have added a new photonic mode, fourth mode, in the system P_3 having resonance frequency ω_{P_3}, corresponding creation (annihilation) operators being $\hat{X}^{\dagger}_{P_3}(\hat{X}_{P_3})$, internal dissipation α_{P_3} and coupling parameter Δ_{MP_3}, $\Delta_{P_1P_3}$ and $\Delta_{P_2P_3}$ for the coupling between MP_3, P_1P_3 and P_2P_3 respectively. Also λ_{P_3} is the strength at which travelling photon waves are driving the mode P_3. The external damping for the mode P_3 is β_{P_3} giving effective damping for the mode $\alpha_{P_3}+\beta_{P_3}$. Following Eq. 5.11 we can write 4×4 coupling matrix as

$$\begin{bmatrix} \tilde{\tilde{\omega}}_M & \Delta_{MP_1}-i\sqrt{\beta_M\beta_{P_1}} & \Delta_{MP_2}-i\sqrt{\beta_M\beta_{P_2}} & \Delta_{MP_3}-i\sqrt{\beta_M\beta_{P_3}} \\ \Delta_{MP_1}-i\sqrt{\beta_M\beta_{P_1}} & \tilde{\tilde{\omega}}_{P_1} & \Delta_{P_1P_2}-i\sqrt{\beta_{P_1}\beta_{P_2}} & \Delta_{P_1P_3}-i\sqrt{\beta_{P_1}\beta_{P_3}} \\ \Delta_{MP_2}-i\sqrt{\beta_M\beta_{P_2}} & \Delta_{P_1P_2}-i\sqrt{\beta_{P_1}\beta_{P_2}} & \tilde{\tilde{\omega}}_{P_2} & \Delta_{P_2P_3}-i\sqrt{\beta_{P_2}\beta_{P_3}} \\ \Delta_{MP_3}-i\sqrt{\beta_M\beta_{P_3}} & \Delta_{P_1P_3}-i\sqrt{\beta_{P_1}\beta_{P_3}} & \Delta_{P_2P_3}-i\sqrt{\beta_{P_2}\beta_{P_3}} & \tilde{\tilde{\omega}}_{P_3} \end{bmatrix}_{4\times4} \tag{5.16}$$

where $\tilde{\tilde{\omega}}_{P_3}=\tilde{\omega}_{P_3}-i\beta_{P_3}=\omega_{P_3}-i(\alpha_{P_3}+\beta_{P_3})$. Complex eigenvalues of this matrix will give complex eigenfrequencies of this hybrid system. The input and output port variables are related to each other, in this case using Eq. 5.7, for four modes we can write P_{out} and P_{in} relation in frequency domain as [Rao et al., 2020; Hu et al., 2022; Shrivastava et al., 2024b]

$$\hat{P}_{out}(\omega)-\hat{P}_{in}(\omega)=-2i\left[\sqrt{\beta_M}\hat{X}_M(\omega)+\sqrt{\beta_{P_1}}\hat{X}_{P_l}(\omega)+\sqrt{\beta_{P_2}}\hat{X}_{P_2}(\omega)+\sqrt{\beta_{P_3}}\hat{X}_{P_3}(\omega)\right] \tag{5.17}$$

For dispersion spectra that takes into account the different types of cooperative effect with all the interactions of magnon mode, photon modes and travelling photon modes of the coupled hybrid system we need to calculate S_{21} (on $\frac{\omega}{2\pi}-H_{dc}$ plane), which following Eq. 5.8 can be written for 1 magnon and 3 photon modes as

$$S_{21}=\frac{\hat{P}_{out}}{\hat{P}_{in}}-1=-\frac{2i}{\hat{P}_{in}}\left[\sqrt{\beta_M}\hat{X}_M+\sqrt{\beta_{P_1}}\hat{X}_{P_1}+\sqrt{\beta_{P_2}}\hat{X}_{P_2}+\sqrt{\beta_{P_3}}\hat{X}_{P_3}\right] \tag{5.18}$$

5.3.2 Results and discussion

The results for this hybrid system are the expected generalisation of the previous case, but we have included it explicitly because this was the precise experimental setup of Bhoi et al. [2022]

Fig. 5.4(a) shows the S_{21} power spectra of the three ISRRs without YIG film. Only three transmission lines horizontal to the applied H_{dc} having resonance frequencies $\omega_{P_1}=3.5$, $\omega_{P_2}=$

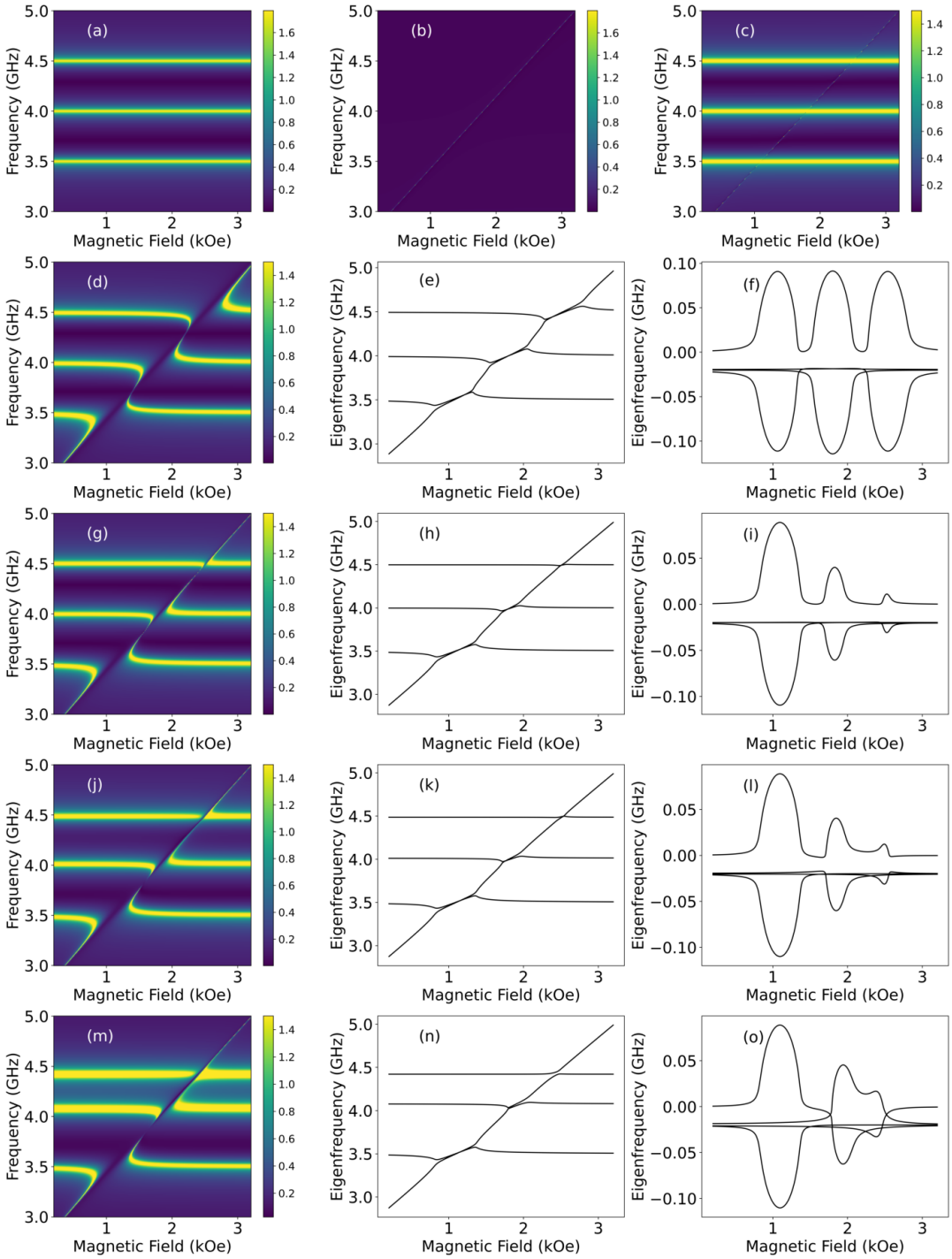

Fig. 5.4 (Caption on next page.)

Fig. 5.4 Hybrid quantum system having 1 TM coupled to 3 SMs. (a) Transmission profile for three static modes, (b) transmission profile for magnon mode, (c) combined transmission profile for three static modes and magnonic mode without any coupling. Transmission profile (d), (e) real, and (f) imaginary part of complex eigenfrequencies, when coupling between TM-2ndSM changed from $0.1i$ to $0.05i$, TM-3rdSM changed from $0.1i$ to $0.02i$. Transmission profile (g), (h) real, and (i) imaginary part of complex eigenfrequencies, when coupling between 2nd-3rdSMs changed from 0 to $0.1i$. Transmission profile (j), (k) real, (l) imaginary part of complex eigenfrequencies, when coupling between 2nd-3rdSMs changed from 0.1 to $0.2i$. The change of parameters are summarized in Table 5.2

Subplots	Δ_{MP_2}	Δ_{MP_3}	$\Delta_{P_2P_3}$	Eigenvalues near MP_3 crossing	
				Real part	imaginary part
d-f	0.1i	0.1i	0i	Attraction	Repulsion
g-i	0.05i	0.02i	0i	Intermediate	Repulsion
j-l	0.01i	0.02i	0.1i	Intermediate	Repulsion
m-o	0.02i	0.2i	0.2i	Repulsion	Attraction

Table 5.2 Set of parameters that are changing and the eigenvalues which are changing qualitatively for Fig. 5.4

4.0 and ω_{P_3}= 4.5 GHz with intrinsic damping rates α_{P_1}= α_{P_2}=α_{P_3}=0.002 [Hu et al., 2022; Rao et al., 2020; Shrivastava et al., 2024b] are visible in the transmission profile on the $(H_{dc} - f_{AC})$ plane which is unaffected by the applied magnetic field. Fig. 5.4(b) showing S_{21} power spectra of the YIG film without ISRRs, having intrinsic damping rate α_M=0.00002 [Bhoi et al., 2022; Bernier et al., 2018; Hu et al., 2022; Rao et al., 2020; Harder et al., 2021; Shrivastava et al., 2024b], showing a slant transmission line which is getting tuned by the applied H_{dc} ranging from 0.2 to 3.2 kOe. Resonance frequency of this FMR (magnon) mode can be linearly modelled as $\omega_M = 0.714 \times H_{dc} + 2.714$ which is varying from 2.856 to 4.998 GHz. Fig. 5.4(c) shows S_{21} power spectra of the two ISRRs and YIG film but without any coupling, which is again a simple addition of Fig. 5.4 (a) and (b) and transmission line of magnon is just crossing the transmission lines of photons.

Fig. 5.4(d, g, j, m) represents transmission profile, Fig. 5.4(e, h, k, n) and Fig. 5.4 (f, i, l, o) represent real and imaginary parts of complex eigenfrequencies respectively. In Fig. 5.4 for each row (d, e, f), (g, h, i), (j, k, l) and (m, n, o) we can divide the each sub-figure in three zones, first zone is for MP_1 around 3.5 GHz ($H_{dc} = 1.1KOe$), second zone is for MP_2 around 4.0 GHz ($H_{dc} = 1.8KOe$) and third zone is for MP_3 around 4.5 GHz ($H_{dc} = 2.5KOe$). For Fig. 5.4(d, e, f), $\Delta_{MP_1} = \Delta_{MP_2} = \Delta_{MP_3} = 0.1i$ and $\Delta_{P_1P_2} = \Delta_{P_1P_3} = \Delta_{P_2P_3} = 0$ so for all

three zones LA in observed in their transmission and real part of complex eigenvalue, and repulsion in their linewidth profile.

For Fig. 5.4(g, h, i) $\Delta_{P_1P_2} = \Delta_{P_1P_3} = \Delta_{P_2P_3} = 0$, $\Delta_{MP_1} = 0.1i$ is not changed although $\Delta_{MP_2} = 0.05i$ and $\Delta_{MP_3} = 0.02i$ is changed, their combined effect on zone 1 getting nullified so the nature of MP_1 interactions remains same. For zone 2 its LA nature in transmission and real part of complex eigenvalue profile have now diminished. Its reduced strength is also visible in their linewidth profile. For zone 3 its LA nature in transmission and real part of complex eigenvalue profile have now diminished to a greater degree and its much reduced strength is also visible in their linewidth profile.

For Fig. 5.4(j, k, l) $\Delta_{MP_3} = \Delta_{P_1P_3} = 0$, $\Delta_{MP_1} = 0.1i$, $\Delta_{MP_2} = 0.05i$ and $\Delta_{MP_3} = 0.02i$ is not changed and only $\Delta_{P_2P_3} = 0$ has changed to $0.1i$. Their combined effect on zone 1 again gets nullified, so the nature of MP_1 interaction remains the same. For zone 2 its LA nature in transmission and real part of the complex eigenvalue profile have now diminished a little more in strength that is also visible in their linewidth profile. For zone 3 the LA nature in transmission and real part of complex eigenvalue profile have now diminished to a greater degree. Its much reduced strength is also visible in their linewidth profile where repulsion is almost washed away and attraction or crossing is just about to start.

For Fig. 5.4(m, n, o) $\Delta_{MP_3} = \Delta_{P_1P_3} = 0$, $\Delta_{MP_1} = 0.1i$, $\Delta_{MP_2} = 0.05i$ and $\Delta_{MP_3} = 0.02i$ is again kept fixed only $\Delta_{P_2P_3} = 0$ has changed to $0.2i$. Their combined effect on zone 1 is again getting nullified so the nature of MP_1 interaction remains the same. For zone 2 the LA nature in transmission and real part of the complex eigenvalue profile have now little more diminished in strength that is also visible in their linewidth profile. For zone 3 the LA nature in transmission and real part of complex eigenvalue profile have ceased and LR has appeared. In their linewidth profile attraction also confirms CIT.

5.4 Conclusion

We have devised a comprehensive quantum theoretical framework for transition between CIA and CIT in a multimode coupled hybrid system which we have shown to work for three and four modes magnon-photon coupled interaction in a planar YIG-ISRRs coupled hybrid system. In a two mode coupled hybrid system the CIA and CIT are determined by dominant dissipative and coherent interactions respectively. Contrary to this in a multimode coupled hybrid system the local CIA / CIT does not only depend on the coupling parameter of the local hybrid modes involved but is a superposition of the all intra and inter coupling parameters of the system. This finding may be utilised to develop new insights for revealing origin of various effects, coupling interactions, and controllable transition between CIA

to CIT and vice versa by manipulation of their coupling strength and dissipation rates etc. Although we have taken examples of magnon-photon coupled hybrid systems, our quantum formalism deals in terms of modes and these modes may be any other real or quasi-particles. This work may also open new experimental and theoretical pathways to explore similar phenomena on the other platforms that will help in advancement of such applications for various quantum devices and materials.